Revealing the role of electron-electron correlations by mapping dissociation of highly excited D_2^+ using ultrashort XUV pulses

L. Martin,[1] R. Y. Bello,[2] C. W. Hogle,[1] A. Palacios,[2,*] X. M. Tong,[3] J. L. Sanz-Vicario,[4] T. Jahnke,[5] M. Schöffler,[5] R. Dörner,[5] Th. Weber,[6] F. Martín,[2,7,8] H. C. Kapteyn,[1] M. M. Murnane,[1] and P. Ranitovic[1,6,9,†]

[1]*JILA and Department of Physics, University of Colorado and NIST, Boulder, Colorado 80309, USA*
[2]*Departamento de Química, Universidad Autónoma de Madrid, Cantoblanco, 28049 Madrid, Spain*
[3]*Center for Computational Sciences, University of Tsukuba, Ibaraki 305-8573, Japan*
[4]*Grupo de Física Atómica y Molecular, Instituto de Física, Universidad de Antioquía, Medellín, Colombia*
[5]*Institut für Kernphysik, University Frankfurt, Max von Laue Strasse 1, D-60438 Frankfurt, Germany*
[6]*Lawrence Berkeley National Laboratory, 1 Cyclotron Road, Berkeley, California 94720, USA*
[7]*Instituto Madrileño de Estudios Avanzados en Nanociencia (IMDEA Nano), Campus de Cantoblanco, 28049 Madrid, Spain*
[8]*Condensed Matter Physics Center (IFIMAC), Universidad Autónoma de Madrid, 28049 Madrid, Spain*
[9]*Laboratorium für Physikalische Chemie, ETH Zürich, 8093 Zürich, Switzerland*

(Received 3 August 2017; published 20 June 2018)

Understanding electron-electron correlations in matter ranging from atoms to solids represents a grand challenge for both experiment and theory. These correlations occur on attosecond timescales and have only recently become experimentally accessible. In the case of highly excited systems, the task of understanding and probing correlated interactions is even greater. In this work, we combine state-of-the-art light sources and advanced detection techniques with *ab initio* calculations to unravel the role of electron-electron correlation in D_2 photoionization by mapping the dissociation of a highly excited D_2^+ molecule. Correlations between the two electrons dictate the pathways along which the molecule dissociates and lead to a superposition of excited ionic states. Using 3D Coulomb explosion imaging and electron-ion coincidence techniques, we assess the relative contribution of competing parent ion states to the dissociation process for different orientations of the molecule with respect to the laser polarization, which is consistent with a shake-up ionization process. As a step toward observing coherent superposition experimentally, we map the relevant nuclear potentials using Coulomb explosion imaging and show theoretically that such an experiment could confirm this coherence via two-path interference.

DOI: 10.1103/PhysRevA.97.062508

I. INTRODUCTION

As the simplest and most abundant molecule in the universe, the hydrogen molecule represents an important test bed for developing a complete understanding of molecular physics on the smallest spatial and fastest vibrational temporal scales. For example, electron double-slit experiments have been performed on the level of a single molecule [1], fast nuclear motions have been observed [2,3], and tests of quantum electrodynamics concepts have been implemented in chemical systems [4]. Ultrafast laser technology and ultrafast high-harmonic pulses enable unprecedented capabilities for capturing and controlling electron dynamics in small atoms, molecules, and materials on femtosecond and even subfemtosecond timescales [5–18]. In parallel with the rapid development of novel ultrafast experimental techniques, full quantum simulations that include correlated electron-electron and electron-nuclear motions have become possible in simple diatomic molecules such as H_2 and D_2.

In this context, extreme ultraviolet (XUV) high-harmonic pulses and infrared (IR) fields have been successfully used to control molecular dissociation of H_2/D_2 after photoionization by steering the reaction with unprecedented precision [19–23]. More recently, coherent attosecond pulse trains in the vacuum UV regime made it possible to coherently control the dynamics of an excited neutral D_2 molecule for the first time [24]. Previously, the dynamics of high-lying electronic states of a hydrogen molecule was out of reach for traditional VUV sources typically used in femtochemistry. Novel applications have also used attosecond XUV techniques to unravel the photoionization delays between direct and the shake-up ionization in atomic targets [25] or to explore the effect of the coupled electron and nuclear motion in hydrogen molecules [26]. In the helium atom, it was found that due to the pure electron-electron correlation effects, the photoionization delays are occurring on a sub-10-attosecond timescale. Trying to progress from a two-electron helium atom to a simple two-electron molecular system and understanding electron-electron correlations in a highly excited hydrogen molecule are particularly challenging from both a theoretical and an experimental point of view. In particular, understanding electron-electron correlations and the coherences in a rapidly dissociating molecular system, where nearly exact theoretical calculations are still tractable, clearly helps us to develop concepts necessary to understand dynamics in more complex molecular systems or correlated materials.

In this work, we combine ultrafast and synchrotron XUV sources with electron-ion 3D coincidence imaging techniques to explore the relevance of electron-electron correlations in the dissociative photoionization of D_2 leading to a highly excited

*Corresponding author: alicia.palacios@uam.es
†Corresponding author: pranitovic@lbl.gov

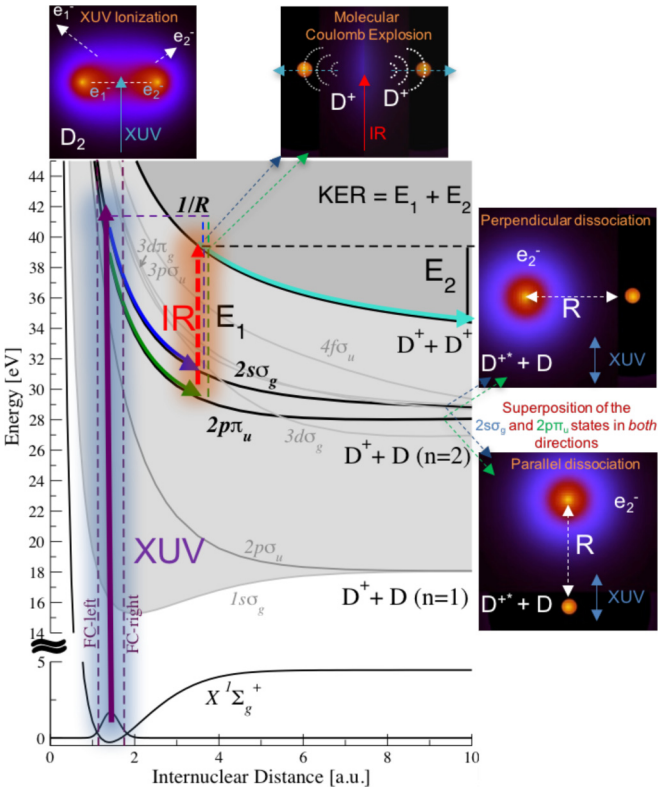

FIG. 1. Correlated electron-electron and nuclear wave packet dynamics in $D_2 + h\nu \rightarrow D_2^+ + e^-$. Ultrashort (and synchrotron) XUV pulses with energy centered at 42.6 eV (42 eV) were used to excite a highly correlated manifold of electronic states in D_2^+. The subsequent dissociative process, following the photoionization, was mapped by using time-resolved IR pulses and Coulomb-explosion imaging. Dashed vertical lines indicate the Franck-Condon boundaries.

D_2^{+*} molecule—the region whose dynamics has not been explored thus far. In particular, we determine the branching ratios for different dissociative ionization channels associated with this molecular shake-up process as a function of the molecular orientation with respect to the laser and XUV polarization. As seen in Fig. 1, a short 42.6 eV high-harmonic pulse first ionizes the neutral molecule, which is hereby excited into high-lying dissociative electronic states of the parent ion. Although most of the D_2^+ molecules are left in the ground state of the ion, a small fraction of them undergoes an excitation-ionization (shake-up) step, where a second electron is excited simultaneously during the photoionization process. Such a process is depicted in the upper-left panel of Fig. 1, and is only possible when the two electrons are tightly correlated [27]. Due to the steep potentials of the highly excited H_2^+ states, the outgoing electron can continuously share the energy with the H_2^{+*} ion left behind. By using a time-delayed infrared probe pulse, combined with electron-ion coincidence imaging techniques, we map the energy distributions of the molecular fragments, which provide an indirect measurement of the nuclear potentials. When combined with advanced *ab initio* calculations that include the coupled nuclear and electronic motions, we draw two significant conclusions. First, we find that the dynamics, captured in the molecular Coulomb explosion (upper-right panel of Fig. 1), is dominated by the excitation of the $2s\sigma_g$ state, regardless of the molecular orientation with respect to the light polarization. The experimental data rule out the naïve model based on a single-active electron picture: one-electron $s \rightarrow p$ dipole transitions within an independent particle model should favor excitation into the $2p\pi_u$ state, particularly for the perpendicular orientation. Second, the dissociation process results in a superposition of nuclear wave packets evolving simultaneously on different potential energy curves of the parent ion, mainly those associated with the $2p\pi_u$ and $2s\sigma_g$ electronic states. Since these states dissociate into the same energy limit, Coulomb imaging of the dissociation process always reflects a mixture of both states. Simulations confirm the presence of coherence and suggest that a similar Coulomb imaging experiment could readily observe it by measuring interference between the $2p\pi_u$ and $2s\sigma_g$ states. Moreover, by using the synchrotron XUV photons of similar energy, we obtain molecular-frame photoelectron angular distributions (MFPADs) showing strong electron-electron correlation effects. In this way, we capture effects that help us fully understand how electron interactions drive the nuclear dynamics in the excitation process of the molecular ion Rydberg states. We offer this time-resolved study of the coupled electron-nuclear dynamics and quantitative analysis of the electron-electron correlation effects that govern the branching ratios for different orientations of the D_2^{+*} molecule dissociating into the $n = 2$ limit.

II. POLARIZATION ORIENTATION EFFECTS IN THE TIME-RESOLVED ELECTRON-NUCLEAR DYNAMICS

We use a 42.6 eV XUV ultrashort pump pulse, synchronized with a probe IR laser (784 nm) to, first, excite and then map the dynamics of the highly excited molecular ion in a COLTRIMS (cold target recoil ion momentum spectroscopy) geometry [28]. The absorption of the XUV pulse ionizes the neutral D_2 molecule, creating a superposition of highly excited electronic states in the molecular ion, as shown in Fig. 1. The excited D_2^{+*} ion can then dissociate along several coherently populated pathways, upon the XUV photoionization, leading to $D^+ + D(n = 1)$ [corresponding to the $D_2^+(1s\sigma_g$ and $2p\sigma_u)$ molecular states] and $D^+ + D(n = 2)$ [corresponding to $D_2^+(2s\sigma_g, 3p\sigma_u, 3d\sigma_g, 2p\pi_u, 3d\pi_g, 4f\sigma_u)$]. Here n is the principle quantum number. As the molecular ion dissociates, with the nuclei following the steep potential energy curves of the D_2^{+*} states, the fragmentation dynamics is mapped by ejecting the second electron using a strong IR laser field. The delayed arrival of the IR pulse interrupts the dissociation process $D_2^{+*} \rightarrow D^+ + D(n)$ at a specific time, by ejecting the second electron and leaving behind two bare deuterons that undergo Coulomb explosion. The latter step is equivalent to projecting the superposition of nuclear wave packets, created by the XUV pulse, onto the Coulombic $1/R$ potential energy curve associated with the doubly ionized molecule (where R is the internuclear separation). The kinetic energy release (KER) and emission direction (parallel or perpendicular to the laser polarization) of the two Coulomb-exploding deuterons is then measured as a function of the XUV-IR time delay.

For the experimental pump-probe setup, we have used a high-power (25 W), high repetition rate (10 kHz) Ti:sapphire laser system coupled to a COLTRIMS coincidence electron-ion detection setup. Most of the laser energy (≈1.7 mJ) was

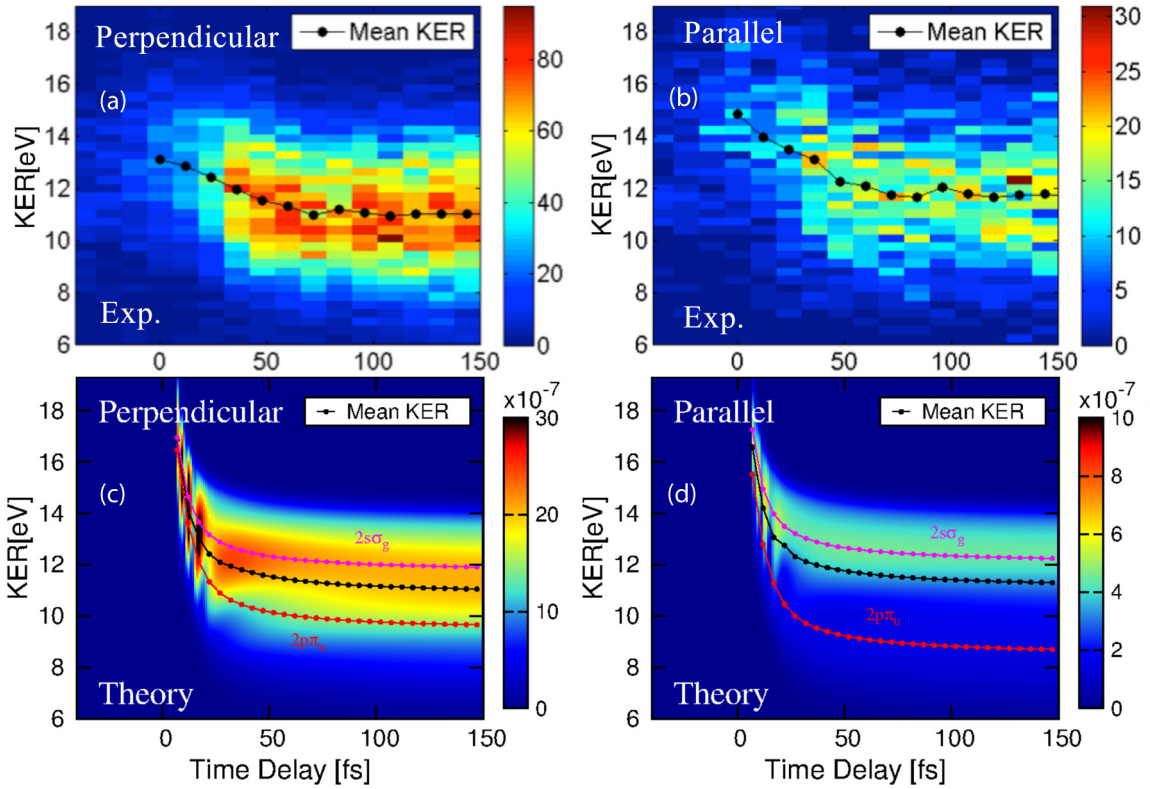

FIG. 2. Measured and calculated dissociative pathways of the highly excited D_2^+ electronic states. (a) and (b) Measured nuclear kinetic energy release (NKE or KER) versus IR time delay for the dissociation events perpendicular and parallel to the XUV/IR polarization direction. The dotted line represents the mean KER of the ion yield for each IR delay value. In the perpendicular case, the coherent superposition of the $2s\sigma_g$ and $2p\pi_u$ dissociative pathways gives a slightly lower mean KER curve compared with the parallel case, where the $2s\sigma_g$ is the largest contribution. (c) and (d) Theoretical calculations for the NKE vs IR time delay with two dissociative pathways, taking into account electron-electron correlation and coupled nuclear wave packet dynamics, for the parallel and perpendicular orientation of the molecule with respect to the light polarization. In (c) and (d) we also include the mean KER corresponding to two truncated simulations where only one individual (incoherent) path is included: $2p\pi_u$ in red dotted line or $2s\sigma_g$ in magenta dotted line.

coupled into a waveguide filled with Ar to generate harmonics, which were then refocused into a supersonic D_2 gas target using a pair of XUV multilayer mirrors, coated to reflect the harmonic centered at 42.6 eV, as shown in Fig. 1. The central photon energies of the harmonics were controlled by tuning the gas pressure in the waveguide, while COLTRIMS enables simultaneous detection of ion and electron 3D momenta [29–31], allowing us to analyze both single and double ionization events in coincidence with electrons, and differentiate various ionization channels. We infer initial molecular orientation relative to the laser polarization from the orientation of the molecular fragments. The residual laser energy was spatially and temporally recombined with the high harmonic beam in a collinear geometry. By using a delay stage with a 10 cm range and a 260 as step size, we could scan from attosecond to femtosecond relative time delays. The duration of the high-harmonic-generation pulse was ≈10 fs, while the IR pulse duration was 30 fs. The probe IR intensity was 5×10^{12} W/cm^2. The IR intensity is strong enough to ionize the excited states of D_2^{+*}, while it is too weak to excite or ionize the ground state of D_2. The electron-ion coincidence experiments were performed at beamline 9.3.2 of the Advanced Light Source synchrotron ring at the Lawrence Berkeley National Laboratory applying the COLTRIMS technique as well. The 3D-vector momenta of the electrons and ions were calculated from the position of impact and the times of flight of each particle; from the momenta the directions and kinetic energies were derived and transformed into the molecular frame. Because of the light electron mass, the electron momentum is about 2.5% of the heavy-particle momentum only, leading to a nearly back-to-back fragmentation of the D^+ ion and D atom, which hence represents the molecular axis at the time of photodissociation.

The measured time-resolved double-ionization yields, which map how the excited molecule dissociates along several potential energy curves, are shown in Fig 2. In Figs. 2(a) and 2(b), we show the experimental KER distribution of the two D^+ ions (originating from the same D_2^{+*} molecule), as a function of the delay between the XUV pump and the IR probe pulses, for the molecules dissociating perpendicular and parallel to the XUV polarization, respectively. In Figs. 2(c) and 2(d) we present the corresponding calculated KERs. The simulation takes into account *both* electron-electron correlation during the ionization process and the coupled nuclear wave packet dynamics during the dissociation. The agreement between experiment and theory depicting the branching ratios of the $2p\pi_u$ and $2s\sigma_g$ states is very good. Additionally, the theory shows quantum beating modes for short time delays. Those are associated with transitions via the $2p\pi_u$ and $2s\sigma_g$ ionic

states that reflect as oscillations in the double-ionization yields for delays of 20–30 fs [see Figs. 2(c) and 2(d)]. For the theoretical simulations, we used an *ab initio* method to describe the interaction with the attosecond XUV pulse. The ionization probabilities for the one-photon absorption process from the ground state of the D_2 molecule are obtained from the exact solution of the time-dependent Schrödinger equation including electron correlation terms and nuclear motion. In brief, the time-dependent wave function is expanded in a basis set of Born-Oppenheimer states, resulting from an L^2 close coupling method. In this expansion, the bound states of D_2 are obtained by performing a configuration interaction calculation in a basis of antisymmetrized products of one-electron functions, and the continuum states are obtained by solving the multichannel scattering equations in a basis of uncoupled continuum states that are written as products of a one-electron wave function for the bound electron and an expansion on spherical harmonics and B-spline functions for the continuum electron. The multichannel expansion includes the six lowest ionic states ($1s\sigma_g$,$2p\sigma_u$,$2p\pi_u$,$2s\sigma_g$,$3d\sigma_g$, and $3p\sigma_u$) and partial waves for the emitted electron up to a maximum angular momentum $l_{\max} = 7$ enclosed in a box of 60 a.u., which amounts up to around 61 000 discretized continuum states. We thus compute the photoionization amplitudes for linearly polarized light for the process $D_2(^1\Sigma_g{}^+) + h\nu \rightarrow [D_2{}^+(nl\lambda_{g,u}) + e_1{}^-(l)]\,{}^1\Lambda_u$, where ${}^1\Lambda_u$ corresponds to the total final symmetry (${}^1\Sigma_u{}^+$ for parallel transitions and ${}^1\Pi_u$ for perpendicular ones). For a given final symmetry, for instance ${}^1\Pi_u$, electrons will be ejected with even angular momenta leaving behind the ion in the $D_2{}^+(2p\pi_u)$ state and odd angular momenta leaving behind the $D_2{}^+(2s\sigma_g)$ state. We have found that the excitation probability for populating doubly excited Q_3 and Q_4 states, which lie in the vicinity of the above $D_2{}^+$ states and autoionize on a femtosecond timescale, was significantly smaller than the probability for ionization + excitation into the states that correlate to the $n = 2$ limit. Thus, the contribution to the total double-ionization yield from these states, in this experiment, is negligible. We have checked that for the electron kinetic energies involved in the single-ionization process considered in this work, the transition amplitudes are converged. We computed the one-photon ionization probabilities after the interaction with a 7 fs duration XUV pulse centered at 42.6 eV (42 eV to compare with the synchrotron radiation simulations) and with an intensity of 10^{12} W/cm^2. Then, the wave packet created in the highly excited ion after interaction with the pump XUV pulse can be written as a coherent sum over vibronic states associated with the $D_2{}^{+*}$ ionic channels $\alpha = 2s\sigma_g$,$3p\sigma_u$,$3d\sigma_g$,$2p\pi_u$,$3d\pi_g$,$4f\sigma_u$, and an electron in the continuum with energy ε_α:

$$\Psi(E,t) = \sum_{\alpha} \sum_{\varepsilon_\alpha} \sum_{\upsilon_\alpha} C_{\alpha,\varepsilon_\alpha,\upsilon_\alpha} e^{-iE_{\varepsilon_\alpha,\upsilon_\alpha}t} \psi_{\alpha,\varepsilon_\alpha}(\mathbf{r},R)\chi_{\upsilon_\alpha}(R). \tag{1}$$

In this expression, the vibronic states with energies $E_{\varepsilon_\alpha,\upsilon_\alpha}$ are descripted as a product of an electronic ($\psi_{\alpha,\varepsilon_\alpha}$) and a nuclear ($\chi_{\upsilon_\alpha}$) wave function, corresponding respectively to the electronic (ε_α) and vibrational (υ_α) continua associated with the α channel. The coefficients $C_{\alpha,\varepsilon_\alpha,\upsilon_\alpha}$ are the accurately computed single-ionization amplitudes. Notice that, for each channel α, the total energy E is shared by both electrons and nuclei. When this wave packet is interrogated by the probe pulse, leading to an emission of the second electron and subsequent Coulomb explosion, different paths leading to the same KER are possible. The action of the delayed IR field to induce the full breakup of the molecule is modeled as a sudden vertical transition in which the $D_2{}^+$ nuclear wave packet is projected onto the $1/R$ potential energy curve of the doubly ionized molecule, using the Franck-Condon (FC) approximation; therefore the KER differential double ionization probability is given by

$$P(\mathrm{KER},t) \propto \sum_{\varepsilon_\alpha} \left| \sum_{\alpha} \sum_{\upsilon_\alpha} \langle \chi_{\upsilon_f} \mid \chi_{\upsilon_\alpha} \rangle e^{-iE_{\varepsilon_\alpha,\upsilon_\alpha}t} C_{\alpha,\varepsilon_\alpha,\upsilon_\alpha} \right|^2. \tag{2}$$

This equation is the result of the following assumptions for the probing step: (i) all electronic dipole couplings between the vibronic states populated by the pump pulse and those populated by the IR pulse are independent of the internuclear distance, and (ii) the energy of the electron emitted by the pump pulse is preserved during the probing step. Both are reasonable approximations for the structureless double electronic continuum that is reached by the combination of the pump and the probe pulses. Equation (2) reveals the relative phases between the vibronic states that conform to the wave packet in (1), giving rise to the observed oscillations in $P(\mathrm{KER},t)$ as a function of t. As all of the α channels contained in the pumped wave packet dissociate into the same limit, $H(n = 2) + H^+$, the amplitude of the oscillations eventually vanishes for longer time delays (as R tends to infinity). The oscillations are not seen in the experimental data mostly because the ionization by the IR probe pulse requires absorption of many photons, a process that connects several dipole matrix elements, and not a simple projection of the $D_2{}^+$ wave packet into the $1/R$ state.

To better see the individual contributions of the wave packets associated with the highly excited ion, in Fig. 3 we plot the KER distributions, i.e., vertical cuts from Fig. 2, for the perpendicular and parallel orientations corresponding to two chosen time delays: 24 fs in the upper panels and 60 fs in the lower panels. We observe a very good agreement between the experimental and theoretical results, with distinct time-dependent KER profiles for different molecular orientation. Note that irrespective of the orientation of the molecule relative to the polarization and the time delay between the two photon pulses, the maximum of the KER distribution does not coincide with the maxima of the individual channels $2p\pi_u$ or $2s\sigma_g$ (yellow and violet full lines in Fig. 3, respectively), which in turn appear at different kinetic energies. On the contrary, the molecule tends to dissociate in a superposition of the $2p\pi_u$ and $2s\sigma_g$ states. For the dissociation in the direction perpendicular to the XUV polarization, the $2s\sigma_g$ and the $2p\pi_u$ states are equally contributing to the overall KER shape. On the other hand, the $2s\sigma_g$ dominates the dissociation in the parallel direction [Fig. 3(b)]. The differences between the $2p\pi_u$ and $2s\sigma_g$ channels are a consequence of the energy and R dependence of the electronic dipole couplings. It is the relative value of these couplings that is at the origin of the actual profiles observed in the double-ionization yields (orange full line in

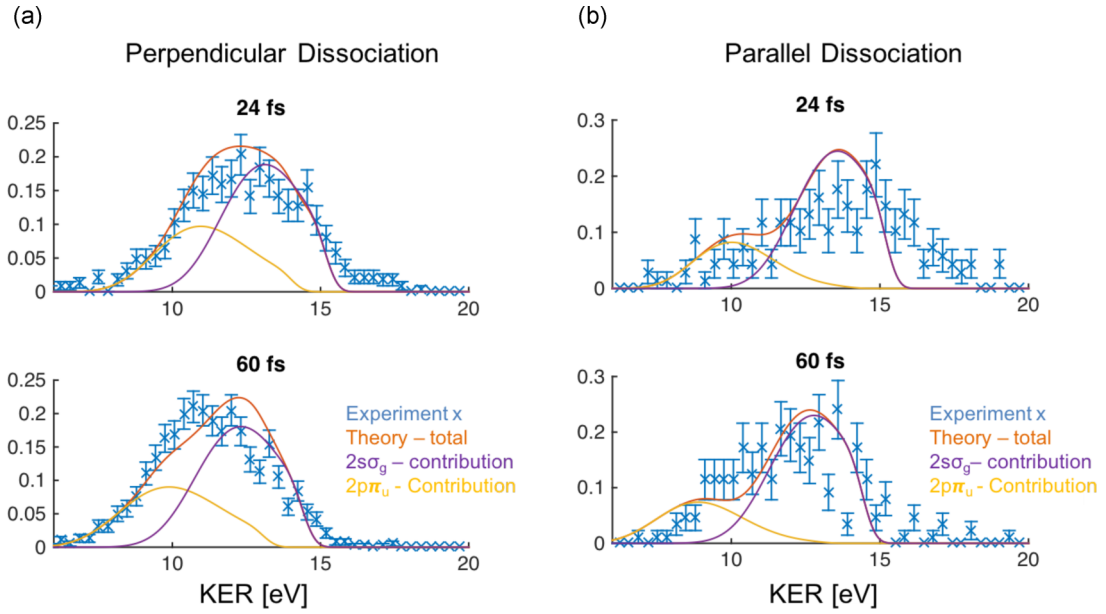

FIG. 3. 1D KER snapshots. (a) Nuclear kinetic energy releases of the Coulomb-exploding molecule at 24 fs and 60 fs delays for the perpendicular dissociation show the snapshots of the dissociative nuclear wave packets at different internuclear distances. Experimental (with error bars) and theoretical data (full orange line). Violet and yellow lines: truncated models including only a single path, through the $2s\sigma_g$ (violet line) or through the $2p\pi_u$ (yellow line). The theory shows that the $2s\sigma_g$ contribution is the largest. (b) Same for the parallel dissociation case, where the $2s\sigma_g$ is again the dominant channel, although the $2p\pi_u$ has a smaller relative contribution. In this case, however, the nuclear wave packet dissociating along the $2p\pi_u$ potential is doing so at higher velocities compared with the parallel case, separating thus faster from the $2s\sigma_g$ states. We note here that even at 60 fs delay, there is still an overlap between the two NWPs.

Fig. 3). This graph suggests that the D^+ yield can be controlled by the combined action of the XUV and the IR pulse (for more details see the Supplemental Material [34]).

The molecular orientation with respect to the light polarization determines not only the yield of the total double-ionization signal, as seen in Fig. 2 by comparing the left and right panels, but also the KER of the fragments obtained after the Coulomb explosion. These polarization-dependent features are solely due to the distinct dynamics initiated by the XUV pump pulse. For each light polarization, a different nuclear wave packet is created with components [dictated by the single-ionization amplitudes in Eq. (1)] that evolve along their corresponding dissociative pathways (see Fig. 1). The dissociation is mostly governed by the coherent excitation of the dominant channels: the $2s\sigma_g$ and $2p\pi_u$ states. Their relevance in the interrupted ultrafast dissociative photoionization of D_2 can be partly disentangled from the measured D^+ yields. The value of the KER for the bare deuterons observed at long time delays already discards the contribution of states correlated with the dissociative channel $D^+ + D(n = 1)$, as schematically depicted in Fig. 1 (KER $= E_1 + E_2$). All the ionic states dissociating into $D^+ + D(n = 2)$ would, however, lead to similar values of the KER, although, as we will further show below, by examining the single-ionization step, their relative weight strongly depends on the molecular orientation.

III. SIGNATURE OF ELECTRON-ELECTRON CORRELATION IN ULTRAFAST MOLECULAR DISSOCIATION AFTER SINGLE IONIZATION

In addition to the time-resolved experiments, we also performed fully differential synchrotron COLTRIMS experiments at a photon energy of 42 eV that reveal the correlated excitation mechanisms in the molecular-frame photoelectron angular distributions (MFPADs) upon single ionization. In Fig. 4(a) we show electron-ion coincidence measurements, averaged over all electron and deuteron angles, which were used to identify the states excited by the XUV pulse. These data are in excellent agreement with those obtained from near-exact theoretical calculations [Fig. 4(d)] that account for electron-electron correlation in the initial ground state as well as in the final states, and during the interaction with the XUV pulse. The photoelectron energies (electron kinetic energies, EKE) were measured in coincidence with the kinetic energy of the D^+ ions (KER) upon dissociative ionization, $D^+ + D(n)$. The signals leading to deuterium atoms in a given n state, $D(n)$, follow the energy-conservation lines defined by KER + EKE $= [h\nu - E_{\mathrm{DIP}(n)}]$, where $h\nu = 42$ eV and $E_{\mathrm{DIP}(n)}$ is the dissociative ionization potential for the $D^+ + D(n)$ channel, namely $E_{\mathrm{DIP}(n=1)} = 18.15$ eV and $E_{\mathrm{DIP}(n=2)} = 28.36$ eV. These energy-conservation values appear along two diagonal lines in Figs. 4(a) and 4(d) and correspond to total energies of ~24 eV for $n = 1$ and ~14 eV for $n = 2$. The contributions of the $1s\sigma_g$ and $2p\sigma_u$ states are clearly distinguishable along the coincidence line for $n = 1$, because a vertical transition from the ground state to each of them leads to a distinct nuclear KER, 0–2 eV and 14–21 eV, respectively. The corresponding signals are weak, which would already explain their minor contribution in the time-resolved experiment (see Fig. 2). Moreover, ejection of the second electron from these channels requires an absorption of a large number of IR photons—much larger than required for ejecting an electron from highly excited states (which lie ~10 eV closer to the double-ionization threshold). Thus, the probability of this process occurring is very unlikely.

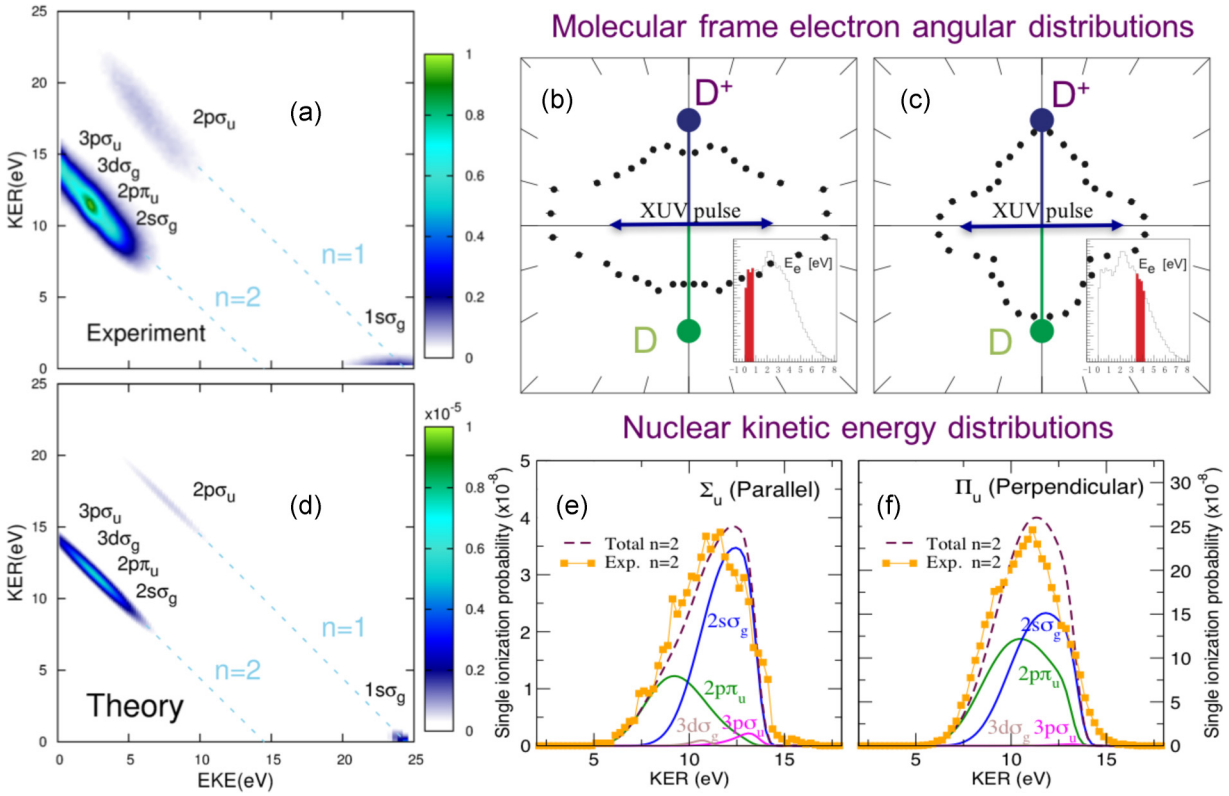

FIG. 4. XUV single ionization probabilities. (a) Nuclear kinetic energy release (KER in y axis) was measured in coincidence with the photoelectron energy (EKE in x axis) using COLTRIMS and 42 eV synchrotron radiation to identify all the channels dissociating in the D($n = 1$) and D($n = 2$) dissociative limit. Contributions from parallel and perpendicular dissociation against the polarization axis are here averaged (see text). Coincidence dashed lines NKE + EKE = [42 − $E_{\mathrm{DIP}(n)}$] (see text) show maximum available energies of ∼24 eV and ∼14 eV for the D($n = 1$) and D($n = 2$) dissociation limits, respectively. (b) and (c) Experimental MFPADs for two different electron energies and the molecular axis fixed perpendicular to the XUV polarization (as indicated by the purple arrows) show the signature of both $D_2{}^+(2s\sigma_g)$ and $D_2{}^+(2p\pi_u)$ electronic states. The insets show the two electron energy slices (∼0.5 eV and ∼4 eV) selected from the broad electron kinetic energy distribution in the region of the D($n = 2$) limit. (d) Theoretical single ionization probabilities computed for a 7 fs XUV pulse centered at 42.6 eV with an intensity $I = 10^{12}$ W/cm^2. As in (a), molecules are randomly oriented with respect to the linearly polarized XUV light. (e) and (f) Calculated (thick dashed line) and renormalized experimental (squares) ion yields for the $D_2{}^{+*} \rightarrow D^+ + D(n = 2)$ dissociation limit for the perpendicular and parallel dissociation directions, integrated over all electron energies. The dominant contributions to the total yield [i.e., dissociative photoionization probabilities for $n = 2$ from (a) and (d) integrated over EKE, in thick dashed line] mostly come from the $D_2{}^+(2s\sigma_g)$ (blue) and $D_2{}^+$ $(2p\pi_u)$ states (green), with the $2s\sigma_g$ state being the main excitation channel in *both* orientations. Higher lying states within the D($n = 2$) manifold barely contribute and only the $D_2{}^+(3p\sigma_u)$ (magenta) and $D_2{}^+(3d\sigma_g)$ (brown) are shown in the figure.

The ionization features of the highly excited states fully overlap along the $n = 2$ coincidence line due to the repulsive character of all the relevant states in the FC region and their degeneracy in the separated-atom limit. All the $D_2{}^{+*}$ states corresponding to D($n = 2$)[$2s\sigma_g$,$3p\sigma_u$,$3d\sigma_g$,$2p\pi_u$,$3d\pi_g$,$4f\sigma_u$] lead to similar electron kinetic energies, ranging from 0 eV to 6 eV, and deuteron energies, from 7 eV to 14 eV, which correspond to the upper and lower limits of the overlap between the ground-state nuclear wave function and the nuclear wave functions associated with the highly excited electronic states in the Franck-Condon region (see Fig. 1). Their relative population for a particular molecular orientation can be partly elucidated by examining the electron angular distributions obtained in the synchrotron radiation experiment [Figs. 4(b) and 4(c)] and are unambiguously determined from the *ab initio* results for the single-ionization probabilities [Figs. 4(e) and 4(f)]. In Figs. 4(b) and 4(c), we show MFPADs for two electron energies (0.5 and 3.5 eV) along the electron-ion coincidence line $n = 2$ for the molecular axis fixed perpendicular to the XUV light polarization direction. Both MFPADs show a significant contribution from electrons ejected perpendicular to the polarization axis. When irradiating a one-active-electron atomic target, photoionization from an s state, using linearly polarized light, leads to a p-wave dipolar emission pattern with a node located at right angles with respect to the polarization axis. In contrast, in a two-active-electron atom such as He, photoionization above the $He^+(n = 2)$ threshold (i.e., excitation + ionization with a single photon), which proceeds through the He($2s\varepsilon p$), He($2p\varepsilon s$), and He($2p\varepsilon d$) channels, may produce a superposition of s, p, and d waves (with more complex nodes) whose components depend on the photoionization branching ratios. For a single-active-electron molecule (e.g., $H_2{}^+$) absorbing linearly polarized light perpendicular to its molecular axis, the dipole selection rules impose that photoionization from the $1s\sigma_g$ state can

only lead to continuum states of π_u symmetry, hence to MFPADs displaying, as in single-active-electron atoms, a nodal plane perpendicular to the polarization vector. This is why the dominant excitation of the $2s\sigma_g$ in Fig. 3(a) was surprising. However, for multiple-active-electron molecular targets, even as simple as D_2, the results of Figs. 4(b) and 4(c) show a significant contribution in the dipole-forbidden region of space. This is caused by the correlation between the ejected photoelectron and the bound electron, which has also been excited by the single XUV photon. Since this bound electron is promoted to a repulsive state of $D_2{}^+$, it acquires a part of the photon energy, but it also acquires part of its angular momentum, while the remaining energy and angular momentum is taken away by the escaping photoelectron [32]. Compared with the time-resolved data [Figs. 2(a), 2(c), and 3(a)], where the excitation probability of the $2s\sigma_g$ and the $2p\pi_u$ states is averaged over all the electron energies in the FC region, the MFPADs in Figs. 4(b) and 4(c) provide additional information for the relative ratios of different electronic channels as a function of the electron energy. From Fig. 1, and the correlation energy diagram shown in Fig. 4(a) ($n = 2$ limit), we see that a low-energy electron is associated with the high-energy D^+ ion in the FC region. Thus, the low-energy-electron MFPAD diagram in Fig. 4(b) can be associated mostly with the upper, $2s\sigma_g$ state, while the MFPAD associated with the high-energy electron [Fig. 4(c)] should be predominantly coming from the lower, $2p\pi_u$ state. However, due to the steep potentials in the FC region, it is obvious that both MFPADs have complex angular distributions with different ratios of the σ_g and the π_u angular characteristics. A similar conclusion can be obtained from the MFPADs with ions dissociating parallel to the XUV polarization. As shown in Figs. 2 and 3, the $2s\sigma_g$ state dominates the dissociation in the parallel direction. Thus, the MFPAD with the most isolated $2s\sigma_g$ character should be coming from the molecule dissociating along the XUV polarization, and should be associated with the low-energy electron. Figure SM4c (in the Supplemental Material [34]) presents such a case, and, indeed, shows the most isotropic electron angular distribution. For a full data set of MFPAD figures for different molecular-axis orientations see the Supplemental Material [34]. In short, whereas the ground state of D_2 can be described as a configuration interaction of the form ${}^1\Sigma_g{}^+[1s\sigma_g(1)1s\sigma_g(2) + \ldots + 2s\sigma_g(1)2s\sigma_g(2) + 2p\pi_u(1)2p\pi_u(2) + \ldots]$, the excitation-ionization states can be described as correlated configurations of the form ${}^1\Sigma_u{}^+[2s\sigma_g(1)\varepsilon s\sigma_u(2) + 2p\pi_u(1)\varepsilon\pi_u(2) + \ldots]$ (parallel orientation) and ${}^1\Pi_u[2s\sigma_g(1)\varepsilon\pi_u(2) + 2p\pi_u(1)\varepsilon\sigma_g(2) + \ldots]$ (perpendicular orientation). Accordingly, while the ionic channels $D_2{}^+(2s\sigma_g)$ and $D_2{}^+(2p\pi_u)$ clearly participate in both orientations, the MFPADs are determined by the partial waves coming from ejected electrons described by $\varepsilon\sigma_u$ and $\varepsilon\pi_g$ states in the parallel case, and $\varepsilon\pi_u$ and $\varepsilon\sigma_g$ states in the perpendicular case. Then the MFPADs cannot be simply analyzed with a one-active-electron model. Compared to the previous work done with lower photon energy, where the molecule dissociates in the $n = 1$ limit [33], these highly differential MFPADs indicate the existence of a strong mixing between the σ and π states of $D_2{}^+$ for both the parallel *and* perpendicular dissociation cases (see also the molecular frame movies in the Supplemental Material [34] for the complete angular dependence picture).

Finally, in Figs. 4(e) (parallel) and 4(f) (perpendicular orientation), we plot the measured and calculated yields of the D^+ ions upon the XUV excitation process in the asymptotic $n = 2$ dissociation limit, integrated over the photoelectron energy. Note that the electron-ion coincidence map, shown in Fig. 4(d) for randomly oriented molecules, is obtained with the weighted average of both orientations (1/3 parallel + 2/3 perpendicular). We include the calculated individual contributions from the four lowest electronic states within the $n = 2$ [$2s\sigma_g$,$3p\sigma_u$,$2p\pi_u$, and $3d\sigma_g$] limit, together with the total yields measured in the synchrotron radiation experiment, confirming that the dominant ionization channels correspond to the $2s\sigma_g$ and $2p\pi_u$ states. The data in Figs. 4(d) and 4(f) are comparable to the long-delay data shown in Fig. 2, where the dissociation process is finished. Similarly to the time-resolved evolution of the dissociative process, the yields of the D^+ ions in the asymptotic dissociative region, shown in Figs. 4(e) and 4(f), immediately reveal that *both* parallel and perpendicular excitations involve the $2s\sigma_g$ and $2p\pi_u$ states, with $2s\sigma_g$ being the main excitation channel in *both* cases. Again, these results cannot be explained by a single-active-electron picture, where only the $2p\pi_u$ state would be populated in a perpendicular transition from the $1s\sigma_g$ state. In contrast, for $n = 1$, i.e., the ionization case where the outgoing electron does not interact with the second electron, a similar one-active-electron picture predicts that the $2p\sigma_u$ state should mainly contribute to the parallel transition, which is in agreement with the results of our *ab initio* calculations.

It is worth noting that before this experiment was done, it was not obvious to us that in both directions of the dissociation, the molecule would be excited in a coherent superposition of the $2s\sigma_g$ and the $2p\pi_u$ states, with different excitation amplitudes of the two electronic states at hand. In our first try, we manifestly failed to reproduce the experimental data shown in Figs. 2(a) and 2(b) by modeling of the dynamics on an assumption that *only* the $2s\sigma_g$ $D_2{}^+$ state is populated for the parallel orientation, and the $2p\pi_u$ state is exclusively populated for the perpendicular one. Only by performing nearly exact calculations, that include the electron-electron correlations in the excitation step, we were able to reproduce the data and show that, for both orientations, the molecule is ionized in a coherent superposition of these two states, with different relative weights of the two electronic states. To the best of our knowledge, this complex shake-up process has not been theoretically discussed in the literature and is far from intuitive since the total excitation probability—which dictates the subsequent rapid dissociation—depends strongly on the electron-electron correlation effects, molecular orientation, and the overlap of the H_2 ground state wave function with the steep $H_2{}^{+*}$ potentials in the Franck-Condon region.

Once the dominant $D_2{}^{+*}$ excitation channels are properly identified, the time-resolved data, shown in Figs. 2 and 3, can be fully understood. First, the relative signal intensity for each molecular orientation is a consequence of the different probabilities for single ionization into the $D_2{}^+$ $2s\sigma_g$ and $2p\pi_u$ states. Both of them are much larger for the perpendicular than for the parallel case [see Figs. 4(e), 4(f)]. Second, the higher asymptotic value of the KER for the parallel case is the result

of the larger population of the D_2^+ $2s\sigma_g$ state [larger, but not dominant; see Figs. 4(e), 4(f)], which lies higher in energy than the D_2^+ $2p\pi_u$ state in the FC region. None of these two features would be observed in the absence of electron-electron correlation either in the D_2 electronic states or during the ionization/excitation process. Ultimately, electron-electron correlation is responsible for changes in the relative population of these states due to changes in the polarization direction of the incoming light, thus leading to a certain degree of control of the D^+ yields under the combined action of the XUV and the IR pulses (see the Supplemental Material [34] for more information).

IV. SUMMARY

In conclusion, we have used perfectly synchronized ultrashort high-harmonic XUV and IR pulses, combined with ion 3D momentum imaging detection techniques, to respectively ionize the D_2 molecule and map the dissociation dynamics of a highly excited D_2^+ molecular ion. We have also used synchrotron radiation and electron-ion coincidence imaging to perform highly differential single-ionization measurements to reveal electron correlation effects as seen in the molecular-frame photoelectron angular distributions. Advanced theory shows that the presence of correlations between the two electrons in D_2 dictates the photoexcitation and the resulting dissociation processes. Due to the highly correlated nature of this process, we have found that the mapping of the rapid XUV-induced dissociation dynamics shows up in the form of a coherent superposition of several electronic states. The quantitative analysis of the correlation effects in this highly excited region of H_2^+ would be important for future attosecond XUV/XUV pump/probe experiments that would allow for measuring of the molecular-frame temporal coherences, as seen in Fig. 2(c). Also, we envision that the use of single-attosecond XUV pulses would allow for perfect control over the localization of the electron wave function in the $n = 2$ dissociative limit.

ACKNOWLEDGMENTS

The authors gratefully acknowledge support from the DOE Office of Basic Energy Sciences (AMOS program, DE-FG02-99ER14982), the Advanced Grant of the ERC XCHEM 290853, the European COST Action XLIC CM1204, and the MINECO Project No. FIS2013-42002-R. J.L.S.V. was supported by Vicerrectoría de Investigación (Estrategia de Sostenibilidad) at Universidad de Antioquia and COLCIENCIAS under Grant No. 111565842968. X.M.T. was supported by a Grand-in-Aid for Scientific Research from the Japan Society for the Promotion of Science. This research used the Advance Light Source and resources of the National Energy Research Scientific Computing Center, DOE Office of Science User Facilities supported by the Director, Office of Science, Office of Basic Energy Sciences, the Division of Chemical Sciences, Geosciences, and Biosciences of the US Department of Energy at LBNL under Contract No. DE-AC02-05CH11231. We acknowledge funding by the Deutsche Forschungsgemeinschaft and DAAD. We thank the staff of the Advanced Light Source, in particular beamline 9.3.2 scientist B. S. Mun for his outstanding support. P.R. thanks RoentDek for their continuous support with the COLTRIMS software and hardware.

[1] D. Akoury, K. Kreidi, T. Jahnke, T. Weber, A. Staudte, M. Schöffler, N. Neumann, J. Titze, L. P. H. Schmidt, A. Czasch, O. Jagutzki, R. A. C. Fraga, R. E. Grisenti, R. Diez Muino, N. A. Cherepkov, S. K. Semenov, P. Ranitovic, C. L. Cocke, T. Osipov, H. Adaniya, J. C. Thompson, M. H. Prior, A. Belkacem, A. L. Landers, H. Schmidt-Böcking, and R. Dörner, Science **318**, 949 (2007).

[2] A. Alnaser, B. Ulrich, X. Tong, I. Litvinyuk, C. Maharjan, P. Ranitovic, T. Osipov, R. Ali, S. Ghimire, Z. Chang, C. Lin, and C. Cocke, Phys. Rev. A **72**, 030702 (2005).

[3] T. Ergler, B. Feuerstein, A. Rudenko, K. Zrost, C. D. Schroter, R. Moshammer, and J. Ullrich, Phys. Rev. Lett. **97**, 103004 (2006).

[4] G. D. Dickenson, M. L. Niu, E. J. Salumbides, J. Komasa, K. S. E. Eikema, K. Pachucki, and W. Ubachs, Phys. Rev. Lett. **110**, 193601 (2013).

[5] M. Drescher, M. Hentschel, R. Kienberger, M. Uiberacker, V. Yakovlev, A. Scrinzi, T. Westerwalbesloh, U. Kleineberg, U. Heinzmann, and F. Krausz, Nature (London) **419**, 803 (2002).

[6] A. L. Cavalieri, N. Mueller, T. Uphues, V. S. Yakovlev, A. Baltuska, B. Horvath, B. Schmidt, L. Bluemel, R. Holzwarth, S. Hendel, M. Drescher, U. Kleineberg, P. M. Echenique, R. Kienberger, F. Krausz, and U. Heinzmann, Nature (London) **449**, 1029 (2007).

[7] L. Miaja-Avila, G. Saathoff, S. Mathias, J. Yin, C. La-o-Vorakiat, M. Bauer, M. Aeschlimann, M. M. Murnane, and H. C. Kapteyn, Phys. Rev. Lett. **101**, 046101 (2008).

[8] E. Gagnon, P. Ranitovic, X.-M. Tong, C. L. Cocke, M. M. Murnane, H. C. Kapteyn, and A. S. Sandhu, Science **317**, 1374 (2007).

[9] M. Schultze, M. Fiess, N. Karpowicz, J. Gagnon, M. Korbman, M. Hofstetter, S. Neppl, A. L. Cavalieri, Y. Komninos, T. Mercouris, C. A. Nicolaides, R. Pazourek, S. Nagele, J. Feist, J. Burgdoerfer, A. M. Azzeer, R. Ernstorfer, R. Kienberger, U. Kleineberg, E. Goulielmakis, F. Krausz, and V. S. Yakovlev, Science **328**, 1658 (2010).

[10] P. Johnsson, J. Mauritsson, T. Remetter, A. L'Huillier, and K. J. Schafer, Phys. Rev. Lett. **99**, 233001 (2007).

[11] P. Ranitovic, X. M. Tong, C. W. Hogle, X. Zhou, Y. Liu, N. Toshima, M. M. Murnane, and H. C. Kapteyn, Phys. Rev. Lett. **106**, 193008 (2011).

[12] E. Turgut, C. La-O-Vorakiat, J. M. Shaw, P. Grychtol, H. T. Nembach, D. Rudolf, R. Adam, M. Aeschlimann, C. M. Schneider, T. J. Silva, M. M. Murnane, H. C. Kapteyn, and S. Mathias, Phys. Rev. Lett. **110**, 197201 (2013).

[13] E. Goulielmakis, Z.-H. Loh, A. Wirth, R. Santra, N. Rohringer, V. S. Yakovlev, S. Zherebtsov, T. Pfeifer, A. M. Azzeer, M. F. Kling, S. R. Leone, and F. Krausz, Nature (London) **466**, 739 (2010).

[14] H. Wang, M. Chini, S. Chen, C.-H. Zhang, F. He, Y. Cheng, Y. Wu, U. Thumm, and Z. Chang, Phys. Rev. Lett. **105**, 143002 (2010).

[15] H. J. Worner, H. Niikura, J. B. Bertrand, P. B. Corkum, and D. M. Villeneuve, Phys. Rev. Lett. **102**, 103901 (2009).

[16] E. Skantzakis, P. Tzallas, J. E. Kruse, C. Kalpouzos, O. Faucher, G. D. Tsakiris, and D. Charalambidis, Phys. Rev. Lett. **105**, 043902 (2010).

[17] M. Holler, F. Schapper, L. Gallmann, and U. Keller, Phys. Rev. Lett. **106**, 123601 (2011).

[18] F. Calegari, D. Ayuso, A. Trabattoni, L. Belshaw, S. De Camillis, S. Anumula, F. Frassetto, L. Poletto, A. Palacios, P. Decleva, J. B. Greenwood, F. Martin, and M. Nisoli, Science **346**, 336 (2014).

[19] F. Kelkensberg, W. Siu, J. F. Perez-Torres, F. Morales, G. Gademann, A. Rouzee, P. Johnsson, M. Lucchini, F. Calegari, J. L. Sanz-Vicario, F. Martin, and M. J. J. Vrakking, Phys. Rev. Lett. **107**, 043002 (2011).

[20] K. P. Singh, F. He, P. Ranitovic, W. Cao, S. De, D. Ray, S. Chen, U. Thumm, A. Becker, M. M. Murnane, H. C. Kapteyn, I. V. Litvinyuk, and C. L. Cocke, Phys. Rev. Lett. **104**, 023001 (2010).

[21] G. Sansone, F. Kelkensberg, J. F. Perez-Torres, F. Morales, M. F. Kling, W. Siu, O. Ghafur, P. Johnsson, M. Swoboda, E. Benedetti, F. Ferrari, F. Lepine, J. L. Sanz-Vicario, S. Zherebtsov, I. Znakovskaya, A. L'Huillier, M. Y. Ivanov, M. Nisoli, F. Martin, and M. J. J. Vrakking, Nature (London) **465**, 763 (2010).

[22] Y. Furukawa, Y. Nabekawa, T. Okino, S. Saugout, K. Yamanouchi, and K. Midorikawa, Phys. Rev. A **82**, 013421 (2010).

[23] A. Fischer, A. Sperl, P. Cörlin, M. Schönwald, H. Rietz, A. Palacios, A. González-Castrillo, F. Martín, T. Pfeifer, J. Ullrich, A. Senftleben, and R. Moshammer, Phys. Rev. Lett. **110**, 213002 (2013).

[24] P. Ranitovic, C. W. Hogle, P. Rivière, A. Palacios, X.-M. Tong, N. Toshima, A. González-Castrillo, L. Martin, F. Martín, and M. M. Murnane, Proc. Natl. Acad. Sci. USA **111**, 912 (2014).

[25] M. Ossiander, F. Siegrist, V. Shirvanyan, R. Pazourek, A. Sommer, T. Latka, A. Guggenmos, S. Nagele, J. Feist, J. Burgdörfer, R. Kienberger, and M. Schultze, Nat. Phys. **13**, 280 (2016).

[26] L. Cattaneo, J. Vos, R. Y. Bello, A. Palacios, S. Heuser, L. Pedrelli, M. Lucchini, C. Cirelli, F. Martin, and U. Keller, Nat. Phys. (2018), doi:10.1038/s41567-018-0103-2.

[27] M. Waitz, R. Y. Bello, D. Metz, J. Lower, F. Trinter, C. Schober, M. Keiling, U. Lenz, M. Pitzer, K. Mertens, M. Martins, J. Viefhaus, S. Klumpp, T. Weber, L. P. H. Schmidt, J. B. Williams, M. S. Schöffler, V. V. Serov, A. S. Kheifets, L. Argenti, A. Palacios, F. Martin, T. Jahnke, and R. Dörner, Nat. Commun. **8**, 2266 (2017).

[28] E. Gagnon, A. S. Sandhu, A. Paul, K. Hagen, A. Czasch, T. Jahnke, P. Ranitovic, C. Lewis Cocke, B. Walker, M. M. Murnane, and H. C. Kapteyn, Rev. Sci. Instrum. **79**, 063102 (2008).

[29] A. Rundquist, C. Durfee, Z. Chang, C. Herne, S. Backus, M. Murnane, and H. Kapteyn, Science **280**, 1412 (1998).

[30] S. Backus, C. G. Durfee III, M. M. Murnane, and H. C. Kapteyn, Rev. Sci. Instrum. **69**, 1207 (1998).

[31] R. Dörner, V. Mergel, O. Jagutzki, L. Spielberger, J. Ullrich, R. Moshammer, and H. Schmidt-Böcking, Phys. Rep. **330**, 95 (2000).

[32] T. Jahnke, J. Titze, L. Foucar, R. Wallauer, T. Osipov, E. P. Benis, O. Jagutzki, W. Arnold, A. Czasch, A. Staudte, M. Schöffler, A. Alnaser, T. Weber, M. H. Prior, H. Schmidt-Böcking, and R. Dörner, J. Electron Spectrosc. Relat. Phenom. **183**, 48 (2011).

[33] A. Lafosse, M. Lebech, J. C. Brenot, P. M. Guyon, L. Spielberger, O. Jagutzki, J. C. Houver, and D. Dowek, J. Phys. B: At., Mol. Opt. Phys. **36**, 4683 (2003).

[34] See Supplemental Material at http://link.aps.org/supplemental/10.1103/PhysRevA.97.062508 for the expanded experimental and theoretical data sets, as well as the MFPADs movies.